Atmos. Chem. Phys. Discuss., 15, 3381–3413, 2015
www.atmos-chem-phys-discuss.net/15/3381/2015/
doi:10.5194/acpd-15-3381-2015
© Author(s) 2015. CC Attribution 3.0 License.

Atmospheric Chemistry and Physics Discussions

This discussion paper is/has been under review for the journal Atmospheric Chemistry and Physics (ACP). Please refer to the corresponding final paper in ACP if available.

Vertical variation of optical properties of mixed Asian dust/pollution plumes according to pathway of airmass transport over East Asia

S.-K. Shin[1], D. Müller[2,*], K. H. Lee[3], D. Shin[4,*], Y. J. Kim[1], and Y. M. Noh[5]

[1]School of Environmental Science and Engineering, Gwangju Institute of Science & Technology (GIST), Gwangju, Republic of Korea
[2]School of Physics, Astronomy and Mathematics, University of Hertfordshire, Hertfordshire, UK
[3]Department of Geoinformatics Engineering, Kyungil University, Gyeongsan, Gyeongbuk, Republic of Korea
[4]Air Quality Forecasting Centre, Climate and Air Quality Research Department, National Institute of Environmental Research, Incheon, Republic of Korea
[5]International Environmental Research Centre (IERC), Gwangju Institute of Science & Technology, Gwangju, Republic of Korea
[*]formerly at: School of Environmental Science and Engineering, Gwangju Institute of Science & Technology, Gwangju, Republic of Korea

Received: 24 December 2014 – Accepted: 21 January 2015 – Published: 6 February 2015

Correspondence to: Y. M. Noh (nym@gist.ac.kr)

Published by Copernicus Publications on behalf of the European Geosciences Union.

ACPD
15, 3381–3413, 2015

Abstract

We use five years (2009–2013) of multiwavelength Raman lidar measurements at Gwangju, Korea (35.10° N, 126.53° E) for the identification of changes of optical properties of East Asian dust in dependence of its transport path over China. Profiles of backscatter and extinction coefficients, lidar ratios, and backscatter-related Ångström exponents (wavelength pair 355/532 nm) were measured at Gwangju. Linear particle depolarization ratios were used to identify East Asian dust layers. We used backward trajectory modelling to identify the pathway and the vertical position of dust-laden air masses over China during long-range transport. Most cases of Asian dust events can be described by the emission of dust in desert areas and subsequent transport over highly polluted regions of China. The Asian dust plumes could be categorized into two classes according to the height above ground in which these plumes were transported: (I) the dust layers passed over China at high altitude levels until arrival over Gwangju, and (II) the Asian dust layers were transported near the surface and the lower troposphere over industrialized areas before they arrived over Gwangju. We find that the optical characteristics of these mixed Asian dust layers over Gwangju differ in dependence of their vertical position above ground over China and the change of height above ground during transport. The mean linear particle depolarization ratio was 0.21 ± 0.06 (at 532 nm), the mean lidar ratios were 52 ± 7 sr at 355 nm and 53 ± 8 sr at 532 nm, and the mean Ångström exponent was 0.74 ± 0.31 in case I. In contrast, plumes transported at lower altitudes (case II) showed low depolarization ratios, and higher lidar ratio and Ångström exponents. The mean linear particle depolarization ratio was 0.13 ± 0.04, the mean lidar ratios were 63 ± 9 sr at 355 nm and 62 ± 8 sr at 532 nm, respectively, and the mean Ångström exponent was 0.98 ± 0.51. These numbers show that the optical characteristics of mixed Asian plumes are more similar to optical characteristics of urban pollution. We find a decrease of the linear depolarization ratio of the mixed dust/pollution plume in dependence of transport time if the pollution layer travelled over China at low heights, i.e., below approximately 3 km above ground. In

ACPD
15, 3381–3413, 2015

contrast we do not find such a trend if the dust plumes travelled at heights above 4 km over China. We need a longer time series of lidar measurements in order to determine the change of optical properties of dust with transport time in a quantitative way.

1 Introduction

Desert dust is the most abundant natural source of atmospheric particles over land. Its light-absorption capacity is comparably strong in the ultraviolet region of the solar spectrum. The transport patterns of dust over North Africa and East Asia as well as the vertical distribution of dust change intra- and inter-annually. Thus the influence of dust on the atmosphere's radiation field is complex (Griggs and Noguer, 2002; Mahowald et al., 2006; Durant et al., 2009). Central East Asia has large desert regions. Asian dust particles that originate from the Taklamakan desert in west China and the Gobi desert in Mongolia and northwest China influence the regional climate over East Asia and can be found as far as the west coast of North America (Husar et al., 2001; McKendry, 2001; Huang et al., 2008). East Asian dust is particularly complicated as it usually travels over densely populated and highly industrialized areas of China before it moves out over Pacific Ocean. During transport over East Asia dust mixes with pollutants such as industrial soot, toxic material, and acidic gases (Sun et al., 2005).

Field campaigns, such as ADEC (Mikami et al., 2006) and ACE-Asia (Huebert et al., 2003) significantly added to our knowledge of the radiative effects of Asian dust. Yu et al. (2006) and Carrico et al. (2003) found differences of dust optical properties as the result of the mixing of dust with anthropogenic pollution between source regions of dust and observation sites downwind of its source regions. The mixing between Asian dust and industrial pollutant particles has significant influence on the size distribution and the chemical composition of Asian dust plumes (Sun et al., 2010; Wang et al., 2007).

There exist few studies on the degree of mixing that occurs between dust and pollution during transport, the effect of the direction of dust transport across China, and the

ACPD
15, 3381–3413, 2015

vertical distribution of Asian dust layers during long-range transport over China. There still is a lack of understanding of how much of the mixing of dust with pollutants depends on the vertical distribution over East Asia when dust passes over source regions of anthropogenic pollution. One reason of our limited knowledge is that there are only few vertically-resolved, long-term observations of pollution over East Asia.

LIDAR (LIght Detection And Ranging) is a powerful technique for measuring the vertical distribution of atmospheric aerosols with high temporal and spatial resolution. In this study we use Raman lidar data taken at Gwangju, South Korea, between 2009 and 2013. In our study we focus specifically on lidar observations of Asian dust layers as they passed over China. We use backward trajectory analysis with HYSPLIT (HYbrid Single Particle Lagrangian Integrated Trajectory) (Draxler and Rolph, 2003) model to identify the transport pathway and the vertical distribution of the Asian dust layers during long-range transport.

The main objective of this study is to investigate the variation of optical properties of mixtures of Asian dust with anthropogenic pollution in dependence of the pathways and vertical distributions of these mixed dust layers during long-range transport. We identify these dust layers by the linear particle depolarization ratio. We present vertically-resolved optical properties such as lidar ratio and Ångström exponent. We also categorize the optical properties of these pollution plumes according to their transport pathway and their vertical distribution.

Section 2 presents the methods used in this study. Section 3 presents our results. We discuss our results and summarize our findings in Sect. 4.

ACPD
15, 3381–3413, 2015

2 Methodology

2.1 GIST Multi-wavelength Raman lidar

The lidar station, dubbed MRS.LEA (Multi-wavelength Raman Spectrometer Lidar in East Asia) of the Gwangju Institute of Science and Technology (GIST) is located at 35.10° N, 126.53° E in the west-south-western part of the Korean peninsula (Fig. 1).

A description of the lidar system is given by Noh et al. (2007, 2008). The system allows us to retrieve vertical profiles of the particle backscatter coefficients at 355, 532, and 1064 nm, the particle extinction coefficients at 355 and 532 nm, the linear particle depolarization ratio at 532 nm, the water-vapor mixing-ratio, and profiles of silicon-dioxide (Müller et al., 2010; Tatarov et al., 2011). Profiles of silicon-dioxide (quartz) can be used as tracer of the concentration of mineral dust. In this contribution we use the signals needed for measuring particle backscatter and extinction coefficients at 355 and 532 nm and the linear particle depolarization ratio.

The profiles of particle backscatter coefficients (β_p) at 355 and 532 nm were calculated with the Raman method (Ansmann et al., 1992). The overlap effect which describes the incomplete overlap between outgoing laser beam and field of view of the receiver telescope is cancelled out for the case of profiles of the backscatter coefficient because the ratios of two signals (elastic signals from particles and molecules and the nitrogen Raman signals) are computed (Wandinger and Ansmann, 2002). In that way we can retrieve vertical profiles of the backscatter coefficient to 400 m above ground. The vertical profiles of the aerosol extinction coefficients (α_p) at 355 and 532 nm were derived with the use of the nitrogen vibration Raman signals at 387 and 607 nm (Ansmann et al., 1990), respectively. We derive particle extinction-to-backscatter ratios (lidar ratios, denoted as S in this contribution) at 355 and 532 nm from the profiles of β_p and α_p. The backscatter-related Ångström exponent for the wavelength pair of 355/532 nm (denoted as $Å_\beta$) is computed, too. The measurements were carried out at nighttime under cloud-free conditions.

ACPD
15, 3381–3413, 2015

Co-polarized and cross-polarized signals are measured at 532 nm. The linear volume depolarization ratio (aerosols + molecules) δ is defined as

$$\delta = \frac{P_\perp}{P_\parallel + P_\perp}. \quad (1)$$

$P_\perp$ and $P_\parallel$ denote the backscatter signal intensities that are polarized perpendicular and parallel with respect to the plane of polarization of the emitted laser beam, respectively.

The linear particle depolarization ratio δ_p differs from δ as it depends on the concentration of particles in relation to the concentration of air molecules. In this contribution we use the linear particle depolarization ratio according to the definition by Shimizu et al. (2004):

$$\delta_p = \frac{\delta(z)R_B(z) - \delta_m}{R_B(z) - 1}. \quad (2)$$

The term δ_m is the linear depolarization ratio of air molecules at the wavelength and bandwidth of the emitted laser wavelength. We used the value $\delta_m = 0.0044$ (Behrendt and Nakamura, 2002). This value takes account of our interference filter which have a full width at half maximum of 1.0 nm. $R_B(z)$ is the backscatter ratio, expressed as $(\beta_p + \beta_m)/\beta_m$ at altitude z. β_m denotes the backscatter coefficient of atmospheric molecules. The calibration of the polarization channels was carried out by using rotating polarizers following the methodology explained by Tesche et al. (2009) and Freudenthaler et al. (2009).

2.2 Dust layer identification

We use the profiles of the depolarization ratio for the identification of the Asian dust layers. An example of how the Asian dust layer was determined is shown in Fig. 2. The Asian dust plume reached Korea on 22 April 2012. Figure 2 shows the time-height

ACPD
15, 3381–3413, 2015

cross section of the range-corrected backscatter signals and the linear volume depolarization ratio at 532 nm. Figure 2 also shows the mean profiles of δ and δ_p, S at 355 and 532 nm, and $Å_\beta$ for the measurement from 13:15 to 14:05 UTC.

Values of δ_p for individual aerosol types are reported in literature, e.g. δ_p for Asian dust particles varies from 0.08–0.35 (Murayama et al., 2004; Shimizu et al., 2004; Chen et al., 2009; Burton et al., 2013; Shin et al., 2013) at 532 nm. Asian dust is generally composed of a mixture of pollution, which leads to variable δ_p. Thus, this range of 0.08–0.35 likely describes mixtures of dust with anthropogenic pollution. For instance, Chen et al. (2009) uses 0.08 as threshold value to identify dust in pollution. Furthermore, optical properties may also change during long-range transport. Shimizu et al. (2004) and Tesche et al. (2011) define 0.1 as threshold value for the determination of aged dust.

In Fig. 2, the layer between 2.7 km 4.6 km (layer II) contains Asian dust particles as suggested from the values of δ_p, which are higher than 0.16. The mean value of δ_p in the layer between 1.2 and 2.5 km (layer I) is 0.11 and thus also points to the presence of dust particles though the concentration of dust particles compared to the concentration of particles of anthropogenic pollution may be lower in layer I compared to layer II.

Other aerosol optical properties in layer I and layer II differ, too. The values of S at 355 and 532 nm in layer I are 64 ± 4 sr and 66 ± 4 sr, respectively. The values of S at 355 and 532 nm in layer II are as low 55 ± 4 sr and 55 ± 3 sr, respectively. The values of $Å_\beta$ in layer I are ~ 0.93 and thus considerably higher than in layer II where we find a value of ~ 0.42. These numbers suggest that layer I might contain a higher concentration of smaller aerosol particles compared to the average particle size in layer II. Regarding the interpretation of the numbers of $Å_\beta$ we need to keep in mind that the backscatter-related Ångström exponent not only depends on particle size but also on the complex refractive index and particle shape. The same holds true for the values of ***S.*** The different numbers thus could also result from differences in particle shape and their absorption properties in these mixed Asian dust layers.

ACPD
15, 3381–3413, 2015

2.3 Analysis of backward trajectories and model simulations of pollution emissions

We used the HYSPLIT (Hybrid Single-Particle Lagrangian Integrated Trajectory) model (Draxler and Rolph, 2003) to generate 120 h backward trajectories for air parcels arriving above our lidar site. The trajectories describe the different altitude levels in which dust was observed during transport. They also allow us to trace back the origin of the dust layers and the transport path.

The Monitoring Atmospheric Composition and Climate (MACC) global air quality service of the European Center for Medium-range Weather Forecasts (ECMWF) provides a reanalysis of global atmospheric composition. The reanalysis assimilates satellite data, e.g. total aerosol optical depth (AOD) which is provided by the Moderate Resolution Imaging Spectroradiometer (MODIS), into a global model and data assimilation system to correct for model departures from observational data (Bellouin, 2013; Inness, 2013). This re-analysis provides fields of aerosols, namely mineral dust, black carbon, organic matter, and sulphate, as well as chemically reactive gases, and greenhouse gases. We used the aerosol AOD from the MACC re-analysis to determine the intensity of pollution (AOD) in densely populated and industrialized regions along the transport path of the dust layers and to investigate the influence of anthropogenic pollution particles on the variation of the optical properties of Asian dust.

3 Results and discussion

We present data that cover the time from 2009–2013. During this time we observed 38 Asian dust layers on 32 days. Figure 3 shows the frequency distribution of δ_p, S, and $Å_\beta$ for the observation period and the transport pathways of each Asian dust plume observed during that time. The average value of δ_p for all observed Asian dust layers is 0.17. The average values of S are 57 sr at 355 nm and 57 sr at 532 nm. The mean value of $Å_\beta$ is 0.84. The depolarization ratios of the Asian dust plume layers of our

ACPD
15, 3381–3413, 2015

study are lower compared to depolarization ratios of pure dust particles. For example, Freudenthaler et al. (2009) report a value of $\delta_p = 0.31$ at 532 nm for Saharan dust observed during SAMUM 2006. Lidar observations were carried out close to the Taklamakan desert (Iwasaka et al., 2003) and the Gobi desert (Yi et al., 2014). We assume that these dust layers exhibit nearly pure dust conditions as anthropogenic pollution sources in these isolated areas are sparse. Values of δ_p are in the range of 0.3 to 0.35 at 532 nm (Iwasaka et al., 2003; Yi et al., 2014). Murayama et al. (2004) find values of $S = 48.6$ sr at 355 nm and $S = 43.1$ sr at 532 in a well-isolated Gobi dust-laden layer observed above 4 km over Tokyo. De Tomasi et al. (2003) report an S value less than 50 sr at 351 nm for a Saharan dust layer. Values of S at 355 nm ranged between 50 and 80 sr for dust observed over Leipzig, Germany (Mattis et al., 2002). The mean value of $\mathring{A}_\beta$ of the dust observed in our study is higher than the value of 0.2 ± 0.2 reported for Saharan dust (Tesche et al., 2009) and ~ 0.3 (Murayama et al., 2002) and 0.4–1.5 (Chen et al., 2007) for Asian dust.

We speculate that the variations of the values of the optical properties of dust particles are caused by the effect of long-range transport and the mixing of dust with anthropogenic pollution or biomass burning smoke when passing over industrialized/densely populated regions in China before they arrived over Korea, see Fig. 3. The transport times suggest that the dust was moderately aged.

3.1 Qualitative analysis of the variation of optical properties of mixed-dust in dependence of pollution levels

We divided the dust layers into two episodes. The two episodes differ according to the level of pollution emissions along the transport pathway of the dust plumes. The separation of our measurements into these two episodes was done on the basis of the distribution of aerosol optical depth. We used model results by MACC and backward trajectory analysis (see Sect. 2.3) for the interpretation of our lidar results as we do not have direct observations of pollution, e.g. particle optical depth, lidar ratios, depolarization ratios, and Ångström exponents along the transport path of the pollution plumes.

ACPD
15, 3381–3413, 2015

There is considerable uncertainty involved in such kind of analysis as it rests upon the interpretation of model results. Nevertheless, our results show a consistent picture and we have confidence that we capture the main features.

Figure 4 shows the distribution of aerosol optical depth (AOD) at 550 nm for dust and anthropogenic pollution on 2 days. These pollutants include organic matter, black carbon, and sulphate aerosol. The pollution AOD was computed with the MACC model using re-analysis data of ECMWF. Figure 4 shows that Asian dust particles emitted from the Taklamakan and the Gobi desert were transported across China. The model results of AOD of anthropogenic pollutants over China for 10 April 2010 is significantly higher than the model results of AOD on 8 March 2013.

On the basis of the distribution of AOD of anthropogenic pollution over China, the Asian dust layers were classified as "more polluted", i.e., "MP" Asian dust when the modelled AOD of anthropogenic pollution on that day was higher than the average AOD (modelled) of all 32 observation days considered in this study. In contrast, Asian dust layers that passed over China during episodes of lower AOD, i.e., AOD was below the mean value of modelled AOD of all 32 observation days are denoted as "less polluted", i.e., "LP" Asian dust.

Figure 5 shows the scatter diagram of $\mathring{A}_\beta$ and S at 355 and 532 nm vs. δ_p in dependence of the transport events denoted as MP and LP. The mean value of δ_p of the Asian dust layers denoted as "LP" cases ranges between 0.08 (threshold value that we use to identify dust) and 0.33. The corresponding values of $\mathring{A}_\beta$ vary between 0.38 and 1.71. The lidar ratios range between 38 and 83 sr at 355 nm and between 41 and 73 sr at 532 nm. The negative correlation of δ_p with $\mathring{A}_\beta$ indicates that the impact of the non-spherical particles (Asian dust with high δ_p) on the backscattered light decreases with increasing $\mathring{A}_\beta$. Higher values of $\mathring{A}_\beta$ indicate a considerable concentration of anthropogenic pollution particles which in turn results in lower values of δ_p, of the mixed dust/pollution plumes.

The values of δ_p tend to decrease when the lidar ratios increase. Lower values of δ_p are connected to lidar ratios above 60–70 sr at 355 and 532 nm. Comparably high lidar

ACPD
15, 3381–3413, 2015

ratios are associated with air masses from urban/industrial areas (Noh et al., 2007; Müller et al., 2007; Burton et al., 2012). We find high values of δ_p for lidar ratios of 57 ± 7 sr at 355 nm and 55 ± 7 sr at 532 nm.

With regard to the MP cases the mean δ_p varies from 0.08 to 0.30. The corresponding values of $Å_\beta$ vary between 0.42 and 1.56. The lidar ratios vary between 44 and 74 sr at 355 nm and between 48 and 72 sr at 532 nm, respectively.

Figure 5d–f shows a negative correlation of δ_p with $Å_\beta$ and S at 355 and 532 nm. The mean values of the LP and MP cases are summarized in Table 1. The transport pathway of dust over eastern China should influence how much anthropogenic aerosols in the industrial areas contribute to the change of optical properties of dust. However, we do not find significant differences between the LP cases and MP cases. We assume that there is another factor that influences the change of the optical properties of the dust layers we observed.

3.2 Influence of pathway and vertical distribution of anthropogenic pollution on optical properties of Asian dust

We classify the Asian dust plumes into 2 categories with regard to height above ground when they passed over regions of anthropogenic emissions during transport. We assume that height above ground influences how much anthropogenic pollution may mix with the dust layers and thus change the optical properties of the dust layers. It is clear that this analysis contains significant uncertainty as (1) model results are used to determine the height of the dust layers above ground during transport over China and (2) we do not have direct measurements of aerosol optical depth along the trajectories of the particle plumes before arrival over Gwangju.

Figure 6 shows the transport pathway and the change of the vertical position of the dust plumes during transport to our lidar site. It is clear that backward trajectories cannot provide us with information on the concentration of dust and anthropogenic pollution in the air masses prior to observation over Korea. Still, backward trajectories

ACPD
15, 3381–3413, 2015

show if the air masses originated from or nearby the desert regions, and whether the air masses passed over densely populated/industrialized regions.

Case I includes those Asian dust plumes that passed over industrialized areas in China at high altitude level (> 3 km height above ground) as shown in Fig. 6a. The Asian dust plumes were classified as Case II when they were transported through the near surface/lower troposphere (< 3 km height above ground) over industrialized areas in China, i.e., longitude range between 110° E and 125° E; the locations of industrialized and densely populated regions in China are shown in Fig. 1. The depolarization ratios of the Asian dust plumes we observed are lower compared to depolarization ratios of pure dust particles. For example, Freudenthaler et al. (2009) report a value of δ_p = 0.31 at 532 nm for pure Saharan dust observed during SAMUM 2006.

The values of δ_p and the corresponding values of $Å_\beta$ and S at 355 and 532 nm for the Cases I and II are also shown in Fig. 6. The corresponding mean values of the parameters of these two cases are summarized in Table 2.

We find different clusters of the optical properties of the dust layers when we take into consideration their vertical position during transport. Cases I show larger values of δ_p compared to case II. On average $Å_\beta$ of case I is smaller than $Å_\beta$ of case II. The average values of δ_p and $Å_\beta$ are 0.21 ± 0.06 and 0.74 ± 0.31, respectively, for case I. In contrast, δ_p and $Å_\beta$ are 0.13 ± 0.04 and 0.98 ± 0.35, respectively, for case II. The lowest values of S at 355 and 532 nm are also measured for high values of δ_p (0.21 ± 0.06). We find values of 52 ± 7 sr at 355 nm and 53 ± 8 sr at 532 nm, respectively, for case I. Comparably high values of S were found for case II, i.e. 63 ± 9 at 355 nm and 62 ± 8 sr at 532 nm. In that case the value of δ_p is 0.13 ± 0.04.

There are several previous studies that report on depolarization ratios of polluted dust after long-range transport. According to these studies the observed dust particles were partly/completely mixed with anthropogenic pollution (Sakai et al., 2002; Müller et al., 2003; Shimizu et al., 2004; Chen et al., 2007). As a result of the mixing of dust with anthropogenic pollution, the values of δ_p were lower than the values of pure dust, which is estimated to be at 0.3–0.35 (Murayama et al., 2004; Freudenthaler et al.,

ACPD
15, 3381–3413, 2015

2009). Likewise, the values of $Å_\beta$ and S also differ compared to the values of $Å_\beta$ and S of pure dust.

We assume that the dust particles carried more anthropogenic pollution in cases where the air masses travelled near the surface. Consequently, the optical characteristics of the dust/pollution layers of case II are dominated by the optical properties of anthropogenic pollutants. In contrast, the optical properties of dust layers that travelled at high altitudes (Case I) are less influenced by urban/industrial pollutants. Thus, the optical properties of these dust layers are more likely to be those of pure dust.

The clusters denoted Case I and Case II were classified according to the altitude the dust-laden air masses passed over industrialized/populated regions of China. The differences of the optical properties of the dust layers are shown in Fig. 7. The corresponding values of the optical characteristics of the Asian dust layers at each individual height are summarized in Table 3. The difference of the optical characteristics of East Asian dust layers that travelled in surface-near heights and at high altitudes is obvious. The values of δ_p, $Å_\beta$ and S are 0.12 ± 0.01, 1.00 ± 0.43, and 63 ± 7 sr at 355 nm and 64 ± 6 sr at 532 nm, respectively, when Asian dust passed over China below 1 km height above ground. These values reflect the fact that the optical properties of the dust/pollution plumes are dominated by the anthropogenic part of the particles in these plumes. In contrast, the values of δ_p, $Å_\beta$, and S were 0.23 ± 0.02, 0.60 ± 027, and 50 ± 7 sr at 355 nm and 49 ± 8 sr at 532 nm, respectively, when the dust layers passed over China at high altitudes, i.e., above 4 km. These values more likely reflect the optical characteristic of Asian dust particles that are less affected by the contribution of anthropogenic pollution.

The altitude in which the Asian dust layers passed over China have significant influence on their optical characteristics. In our study, we took 3 km above ground as threshold value as we observed a notable change of optical properties of the dust/pollution plumes if they travelled below or below 3 km height above ground. Pollution particles below 3 km could mix and interact with Asian dust particles (more influence). In contrast, we assume that optical properties of dust particles above 3 km are not that much

ACPD
15, 3381–3413, 2015

influenced by anthropogenic pollution as the mixing of pollution into these heights is less intense. This height of 3 km is also in relatively good agreement with the average height of planetary boundary layers. Pollutants emitted at the surface predominantly stay in this height (Basha et al., 2009).

We emphasize that this threshold value of 3 km is merely a best estimate which is governed by the set of data we have at hand. We lack in additional information that would allow us to refine our data analysis, as for example a longer time series of lidar measurements, (vertically resolved) observations of pollution transported over China, measurements under much more variable meteorological conditions, additional modelling results, just to name a few reasons, might change this threshold value.

Figure 8 shows scatter diagrams of optical properties of Asian dust vs. the transport time. The correlation study is based on HYSPLIT model results, our profiles of δ_{p}, $\mathring{A}_{\beta}$, and S, and the time (in hours) the Asian dust spent in polluted regions over China during the transport. We can only use HYPLIT results as an estimate of the total transport time and the time the plumes spent over pollution regions of China. The total transport time may have considerable uncertainty. We need to decide from the trajectories the start point of dust emission and this means we take the time when the air parcel (defined by its trajectory) left one of the desert regions in Central Asia. The height above ground during transport and the time the plumes spent over pollution regions also contains uncertainty as we neither have direct measurements of the height distribution of the plumes over China during transport nor we have information on the pollution levels over China while the desert plumes travelled over China in the various height layers. We can merely assume that the likelihood of mixing with dust and pollution increases the lower the dust travels above ground and the longer it travels at low heights.

We again used our classification of Case I and Case II. However, we refined the vertical resolution to 5 height layers, i.e. transport occurred below 1 km, from 1–2 km, from 2–3 km, from 3–4 km, and above 4 km. We wanted to test if a more refined height separation would give as more insight on the change of optical properties with transport time and transport height.

ACPD
15, 3381–3413, 2015

The absolute time the dust layers spent in these different height levels is presented in Fig. 8. We also tested the effect of relative time in relation to total transport time but could not find a clear pattern. We find a maximum value of 0.3 for δ_p at 532 nm. On average, the depolarization decreases with increasing residence time over China. However, this dependence seems mainly driven by the fact that the depolarization ratio of particles above 3 km is larger and describes plumes with considerably shorter residence times (fast transport) than the factor 2 longer residence times of plumes below 3 km height above ground.

Regarding $Å_\beta$ we find a maximum value of 1.75 which decreases to 0.5 for plumes with transport times of 50 h. The decrease of $Å_\beta$ with transport time seems to show a correlation for plumes that mainly stay below 3 km height above ground. In contrast, plumes above 3 km do not seem to change $Å_\beta$ with transport time, which may either be related to the short transport times of less than 20 h or the fact that mixing of pollution with dust is less likely to happen if the dust plumes travel above 3 km above ground.

With regard to S at 355 and 532 nm we find a maximum value of approximately 75 sr which drops to approximately 40 sr for transport times of 50 h. Again, we see that for plumes below 3 km height above ground transport time seems to matter. S drops with increasing transport time. For the case of plumes above 3 km, i.e. dust that likely is not too much affected by mixing with anthropogenic pollution, the lidar ratios do not seem to depend on transport time. This result may however again be caused by the fact that transport times to Korea are comparably short, i.e. 20 h or less.

We will further investigate these results. We initially assumed that $Å_\beta$ should increase with transport time, or do not drop that significantly, for pollution that travels near the ground as they should be a higher share of small anthropogenic pollution particles in the dust plume (large particles). This opposite behaviour may be caused by the state of mixing, i.e., pollution particles attach to the dust particles, thus increasing their mean size. Hygroscopic growth of particles attached to dust may further contribute to the increase of mean size. One point that complicates this interpretation is that $Å_\beta$ do not

ACPD
15, 3381–3413, 2015

only depend on particle size but also on particle shape and the real and imaginary part (scattering and absorption) of the particles.

With regard to S we also expected that S would increase with increasing transport times. If the particles travel at low height above ground more anthropogenic pollution should mix into the dust plumes. The decrease of S however suggests an increase of particle size and a decrease of the light-absorption capacity. Hygroscopic particle growth, i.e. increase of mean particle size and decrease of light-absorption by uptake of water might be responsible for this behavior.

We stress that other reasons may be responsible for these results. We have a comparably small set of observations. We have insufficient information whether the plumes consisted of internal and/or external mixtures. The shape and size of particles of mixed Asian dust might be influenced more by transport time. Internal/external mixing between the dust particles and pollution particles, could influence the light-absorption properties.

4 Summary and conclusion

In this study we presented the differences of optical properties of mixed Asian dust layers in dependence of their vertical position over China during transport from the Chinese dust source regions to Korea. The data cover the time frame from 2009–2013. The dust layers are divided into several categories which can be characterized by different heights above ground during transport. The change of height above ground during transport of the dust layers was identified by backward trajectory analysis.

The optical properties of Asian dust significantly change in dependence of the dust plumes, the vertical position, and the change of vertical position above ground level during transport over China. We find lower values of the lidar ratios at 355 and 532 nm, lower backscatter-related Ångström exponents (wavelength pair 355/532 nm), and higher linear particle depolarization ratios at 532 nm for Asian dust that was transported at high altitudes compared to the situation in which the dust plumes moved at

ACPD
15, 3381–3413, 2015

low altitudes across China. The mean linear particle depolarization ratio is 0.21 ± 0.06 for transport at high altitudes. The mean lidar ratios in that case are 52 ± 7 sr and 53 ± 8 sr at 355 and 532 nm, respectively. The mean Ångström exponent is 0.74 ± 0.31. These values likely reflect properties of dust little affected by anthropogenic pollution. However, we cannot quantify the amount of anthropogenic pollution that may still be present in these dust layers. In contrast, higher values of the lidar ratios and the backscatter-related Ångström exponents, and lower values of the linear particle depolarization were found for dust layers that crossed highly polluted regions in China at low altitudes. The value of the mean linear particle depolarization ratio is 0.13 ± 0.04. The mean lidar ratios are 63 ± 9 sr and 62 ± 8 sr at 355 and 532 nm, respectively. The mean backscatter-related Ångström exponent is 0.98 ± 0.35. These values more likely describe strong influence by anthropogenic pollution, i.e. the uptake of urban pollution by dust may have been significant.

Our results suggest that the transport pathway as well as the vertical position of Asian dust during long-range transport may have significant impact on the optical properties of mixed Asian dust layers.

Acknowledgements. This work was supported by a National Research Foundation of Korea (NRF) grant funded by the Korean government (MEST) (No. 2012R1A1A2002983) and the Eco-Innovation Project 2012000160004 from Korean Ministry of Environment through the Advanced Environmental Monitoring Research Center.

References

Ansmann, A., Riebesell, M., and Weitkamp, C.: Measurement of atmospheric aerosol extinction profiles with a Raman lidar, Opt. Lett., 15, 746–748, 1990.

Ansmann, A., Wandinger, U., Riebesell, M., Weitkamp, C., and Michaelis, W.: Independent measurement of extinction and backscatter profiles in cirrus clouds by using a combined Raman elastic-backscatter lidar, Appl. Optics, 31, 7113–7131, 1992.

Basha, G. and Ratnam, M. V.: Identification of atmospheric boundary layer height over a tropical station using high-resolution radiosonde refractivity profiles: compari-

ACPD
15, 3381–3413, 2015

son with GPS radio occultation measurements, J. Geophys. Res.-Atmos., 114, D16101, doi:10.1029/2008JD011692, 2009.
Behrendt, A. and Nakamura, T.: Calculation of the calibration constant of polarization lidar and its dependency on atmospheric temperature, Opt. Express, 10, 805–817, 2002.
Bellouin, N., Quaas, J., Morcrette, J.-J., and Boucher, O.: Estimates of aerosol radiative forcing from the MACC re-analysis, Atmos. Chem. Phys., 13, 2045–2062, doi:10.5194/acp-13-2045-2013, 2013.
Burton, S. P., Ferrare, R. A., Hostetler, C. A., Hair, J. W., Rogers, R. R., Obland, M. D., Butler, C. F., Cook, A. L., Harper, D. B., and Froyd, K. D.: Aerosol classification using airborne High Spectral Resolution Lidar measurements – methodology and examples, Atmos. Meas. Tech., 5, 73–98, doi:10.5194/amt-5-73-2012, 2012.
Burton, S. P., Ferrare, R. A., Vaughan, M. A., Omar, A. H., Rogers, R. R., Hostetler, C. A., and Hair, J. W.: Aerosol classification from airborne HSRL and comparisons with the CALIPSO vertical feature mask, Atmos. Meas. Tech., 6, 1397–1412, doi:10.5194/amt-6-1397-2013, 2013.
Carrico, C. M., Kus, P., Rood, M. J., Quinn, P. K., and Bates, T. S.: Mixtures of pollution, dust, sea salt, and volcanic aerosol during ACE-Asia: radiative properties as a function of relative humidity, J. Geophys. Res.-Atmos., 108, 8650, doi:10.1029/2003JD003405, 2003.
Chen, W.-N., Tsai, F.-J., Chou, C. C.-K., Chang, S.-Y., Chen, Y.-W., and Chen, J.-P.: Optical properties of Asian dusts in the free atmosphere measured by Raman lidar at Taipei, Taiwan, Atmos. Environ., 41, 7698–7714, 2007.
Chen, W.-N., Chen, Y.-W., Chou, C. C., Chang, S.-Y., Lin, P.-H., and Chen, J.-P.: Columnar optical properties of tropospheric aerosol by combined lidar and sunphotometer measurements at Taipei, Taiwan, Atmos. Environ., 43, 2700–2708, 2009.
De Tomasi, F., Blanco, A., and Perrone, M. R.: Raman lidar monitoring of extinction and backscattering of African dust layers and dust characterization, Appl. Optics, 42, 1699–1709, 2003.
Draxler, R. R. and Rolph, G.,: HYSPLIT (Hybrid Single-Particle Lagrangian Integrated Trajectory) model access via NOAA ARL READY website, NOAA Air Resources Laboratory, Silver Spring, MD, available at: http://www.arl.noaa.gov/ready/hysplit4.html (last access: October 2014), 2003.
Durant, A. J., Harrison, S. P., Watson, I. M., and Balkanski, Y.: Sensitivity of direct radiative forcing by mineral dust to particle characteristics, Prog. Phys. Geog., 33, 80–102, 2009.

ACPD
15, 3381–3413, 2015

Freudenthaler, V., Esselborn, M., Wiegner, M., Heese, B., Tesche, M., Ansmann, A., Müller, D., Althausen, D., Wirth, M., and Fix, A.: Depolarization ratio profiling at several wavelengths in pure Saharan dust during SAMUM 2006, Tellus B, 61, 165–179, 2009.

Griggs, D. J. and Noguer, M.: Climate change 2001: the scientific basis, Contribution of working group I to the third assessment report of the intergovernmental panel on climate change, Weather, 57, 267–269, 2002.

Huang, J., Minnis, P., Chen, B., Huang, Z., Liu, Z., Zhao, Q., Yi, Y., and Ayers, J. K.: Long-range transport and vertical structure of Asian dust from CALIPSO and surface measurements during PACDEX, J. Geophys. Res.-Atmos., 113, D23212, doi:10.1029/2008JD010620, 2008.

Huebert, B. J., Bates, T., Russell, P. B., Shi, G., Kim, Y. J., Kawamura, K., Carmichael, G., and Nakajima, T.: An overview of ACE-Asia: strategies for quantifying the relationships between Asian aerosols and their climatic impacts, J. Geophys. Res.-Atmos., 108, 8633, doi:10.1029/2003JD003550, 2003.

Husar, R. B., Tratt, D., Schichtel, B. A., Falke, S., Li, F., Jaffe, D., Gasso, S., Gill, T., Laulainen, N. S., and Lu, F.: Asian dust events of April 1998, J. Geophys. Res.-Atmos., 106, 18317–18330, 2001.

Inness, A., Baier, F., Benedetti, A., Bouarar, I., Chabrillat, S., Clark, H., Clerbaux, C., Coheur, P., Engelen, R., and Errera, Q.: The MACC reanalysis: an 8 yr data set of atmospheric composition, Atmos. Chem. Phys., 13, 4073–4109, 2013, http://www.atmos-chem-phys.net/13/4073/2013/.

Iwasaka, Y., Shibata, T., Nagatani, T., Shi, G. Y., Kim, Y., Matsuki, A., Trochkine, D., Zhang, D., Yamada, M., and Nagatani, M.: Large depolarization ratio of free tropospheric aerosols over the Taklamakan Desert revealed by lidar measurements: possible diffusion and transport of dust particles, J. Geophys. Res.-Atmos., 108, 8652, doi:10.1029/2002JD003267, 2003.

Mahowald, N. M., Muhs, D. R., Levis, S., Rasch, P. J., Yoshioka, M., Zender, C. S., and Luo, C.: Change in atmospheric mineral aerosols in response to climate: last glacial period, preindustrial, modern, and doubled carbon dioxide climates, J. Geophys. Res.-Atmos., 111, D10202, doi:10.1029/2005JD006653, 2006.

Mattis, I., Ansmann, A., Müller, D., Wandinger, U., and Althausen, D.: Dual-wavelength Raman lidar observations of the extinction-to-backscatter ratio of Saharan dust, Geophys. Res. Lett., 29, 20-21–20-24, 2002.

ACPD
15, 3381–3413, 2015

McKendry, I., Hacker, J., Stull, R., Sakiyama, S., Mignacca, D., and Reid, K.: Long-range transport of Asian dust to the Lower Fraser Valley, British Columbia, Canada, J. Geophys. Res.-Atmos., 106, 18361–18370, 2001.

Mikami, M., Shi, G., Uno, I., Yabuki, S., Iwasaka, Y., Yasui, M., Aoki, T., Tanaka, T., Kurosaki, Y., and Masuda, K.: Aeolian dust experiment on climate impact: an overview of Japan–China joint project ADEC, Global Planet. Change, 52, 142–172, 2006.

Müller, D., Franke, K., Ansmann, A., Althausen, D., and Wagner, F.: Indo-Asian pollution during INDOEX: microphysical particle properties and single-scattering albedo inferred from multiwavelength lidar observations, J. Geophys. Res.-Atmos., 108, 4600, doi:10.1029/2003JD003538, 2003.

Müller, D., Ansmann, A., Mattis, I., Tesche, M., Wandinger, U., Althausen, D., and Pisani, G.: Aerosol-type-dependent lidar ratios observed with Raman lidar, J. Geophys. Res.-Atmos., 112, D16202, doi:10.1029/2006JD008292, 2007.

Müller, D., Mattis, I., Tatarov, B., Noh, Y., Shin, D., Shin, S., Lee, K., Kim, Y., and Sugimoto, N.: Mineral quartz concentration measurements of mixed mineral dust/urban haze pollution plumes over Korea with multiwavelength aerosol Raman-quartz lidar, Geophys. Res. Lett., 37, L20810, doi:10.1029/2010GL044633, 2010.

Murayama, T.: Optical properties of Asian dust aerosol lofted over Tokyo observed by Raman lidar, Lidar Remote Sensing in Atmospheric and Earth Sciences, edited by: Bissonnette, L. R., Roy, G., and Vallée, G., Defence R&D Canada, Val-Bélair, 1, 331–334, 2002.

Murayama, T., Müller, D., Wada, K., Shimizu, A., Sekiguchi, M., and Tsukamoto, T.: Characterization of Asian dust and Siberian smoke with multi-wavelength Raman lidar over Tokyo, Japan in spring 2003, Geophys. Res. Lett., 31, L23103, doi:10.1029/2004GL021105, 2004.

Noh, Y. M., Kim, Y. J., Choi, B. C., and Murayama, T.: Aerosol lidar ratio characteristics measured by a multi-wavelength Raman lidar system at Anmyeon Island, Korea, Atmos. Res., 86, 76–87, 2007.

Noh, Y. M., Kim, Y. J., and Müller, D.: Seasonal characteristics of lidar ratios measured with a Raman lidar at Gwangju, Korea in spring and autumn, Atmos. Environ., 42, 2208–2224, 2008.

Sakai, T., Shibata, T., Iwasaka, Y., Nagai, T., Nakazato, M., Matsumura, T., Ichiki, A., Kim, Y.-S., Tamura, K., and Troshkin, D.: Case study of Raman lidar measurements of Asian dust events in 2000 and 2001 at Nagoya and Tsukuba, Japan, Atmos. Environ., 36, 5479–5489, 2002.

ACPD
15, 3381–3413, 2015

Shimizu, A., Sugimoto, N., Matsui, I., Arao, K., Uno, I., Murayama, T., Kagawa, N., Aoki, K., Uchiyama, A., and Yamazaki, A.: Continuous observations of Asian dust and other aerosols by polarization lidars in China and Japan during ACE-Asia, J. Geophys. Res.-Atmos., 109, D19S17, doi:10.1029/2002JD003253, 2004.

Shin, S., Müller, D., Kim, Y., Tatarov, B., Shin, D., Seifert, P., and Noh, Y. M.: The retrieval of the Asian dust depolarization ratio in Korea with the correction of the polarization-dependent transmission, Asia-Pacific, J. Atmos. Sci., 49, 19–25, 2013.

Sun, Y., Zhuang, G., Wang, Y., Zhao, X., Li, J., Wang, Z., and An, Z.: Chemical composition of dust storms in Beijing and implications for the mixing of mineral aerosol with pollution aerosol on the pathway, J. Geophys. Res.-Atmos., 110, D24209, doi:10.1029/2005JD006054, 2005.

Sun, Y., Zhuang, G., Huang, K., Li, J., Wang, Q., Wang, Y., Lin, Y., Fu, J. S., Zhang, W., and Tang, A.: Asian dust over northern China and its impact on the downstream aerosol chemistry in 2004, J. Geophys. Res.-Atmos., 115, D00K09, doi:10.1029/2009JD012757, 2010.

Tatarov, B., Müller, D., Shin, D. H., Shin, S. K., Mattis, I., Seifert, P., Noh, Y. M., Kim, Y., and Sugimoto, N.: Lidar measurements of Raman scattering at ultraviolet wavelength from mineral dust over East Asia, Opt. Express, 19, 1569–1581, 2011.

Tesche, M., Ansmann, A., Müller, D., Althausen, D., Mattis, I., Heese, B., Freudenthaler, V., Wiegner, M., Esselborn, M., and Pisani, G.: Vertical profiling of Saharan dust with Raman lidars and airborne HSRL in southern Morocco during SAMUM, Tellus B, 61, 144–164, 2009.

Tesche, M., Müller, D., Gross, S., Ansmann, A., Althausen, D., Freudenthaler, V., Weinzierl, B., Veira, A., and Petzold, A.: Optical and microphysical properties of smoke over Cape Verde inferred from multiwavelength lidar measurements, Tellus B, 63, 677–694, 2011.

Wandinger, U. and Ansmann, A.: Experimental determination of the lidar overlap profile with Raman lidar, Appl. Optics, 41, 511–514, 2002.

Wang, Y., Zhuang, G., Tang, A., Zhang, W., Sun, Y., Wang, Z., and An, Z.: The evolution of chemical components of aerosols at five monitoring sites of China during dust storms, Atmos. Environ., 41, 1091–1106, 2007.

Yi, B., Yang, P., and Baum, B. A.: Impact of pollution on the optical properties of trans-Pacific East Asian dust from satellite and ground-based measurements, J. Geophys. Res.-Atmos., 119, 5397–5409, doi:10.1002/2014JD021721, 2014.

Yu, X., Cheng, T., Chen, J., and Liu, Y.: A comparison of dust properties between China continent and Korea, Japan in East Asia, Atmos. Environ., 40, 5787–5797, 2006.

ACPD
15, 3381–3413, 2015

Table 1. Linear particle depolarization ratio at 532 nm, lidar ratios, and backscatter-related Ångström exponents of Asian dust layers for different levels of anthropogenic pollution emissions.

	Number of observed layers	Depolarization ratio	Lidar ratio 355 nm	Lidar ratio 532 nm	Ångström exponent
Less polluted	25	0.17 ± 0.02	57 ± 7	55 ± 7	0.82 ± 0.37
More polluted	13	0.17 ± 0.2	58 ± 6	59 ± 8	0.89 ± 0.38

ACPD
15, 3381–3413, 2015

Table 2. Summary of the linear particle depolarization ratio at 532 nm, the lidar ratio, and the backscatter Ångström exponents of Asian dust layers for Case I, i.e., Asian dust layers passed over China at high altitude (> 3 km) before they arrived over Gwangju, and Case II, i.e., Asian dust layers were transported at low altitude (< 3 km) over industrialized areas before they arrived over Gwangju.

Vertical position at pollution regions	Number of observed layers	Depolarization ratio	Lidar ratio 355 nm	Lidar ratio 532 nm	Ångström exponent
Case I	16	0.21 ± 0.06	52 ± 7	53 ± 8	0.74 ± 0.31
Case II	22	0.13 ± 0.04	63 ± 9	62 ± 8	0.98 ± 0.35

ACPD
15, 3381–3413, 2015

Table 3. Linear particle depolarization ratio at 532 nm, lidar ratios, and backscatter-related Ångström exponents of East Asian dust layers according to altitude range in which these plumes passed over polluted regions of China. Case I describes the layer from 3–4 km and above 4 km. Case II describes the layers from 0–1 km, from 1–2 km, and from 2–3 km height.

Height of dust layer at pollution regions		Number of observed layers	Depolarization ratio	Lidar ratios 355 nm	Lidar ratios 532 nm	Ångström exponent
Case I	Above 4 km	14	0.23 ± 0.02	50 ± 7	49 ± 8	0.60 ± 0.27
	3–4 km	1	0.20 ± 0.04	44 ± 2	47 ± 7	0.67 ± 0.29
Case II	2–3 km	7	0.13 ± 0.02	61 ± 7	66 ± 5	1.11 ± 0.47
	1–3 km	6	0.15 ± 0.03	65 ± 7	59 ± 9	0.94 ± 0.42
	Below 3 km	10	0.12 ± 0.01	63 ± 7	64 ± 6	1.00 ± 0.43

ACPD
15, 3381–3413, 2015

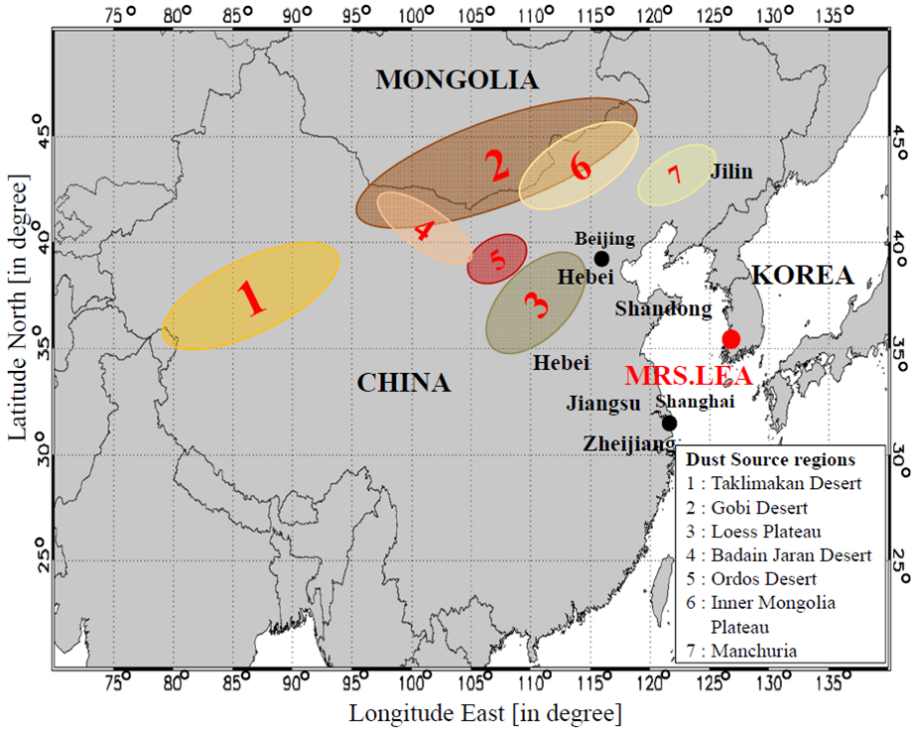

Figure 1. Map of the desert and loess regions. The location of some major cities (Beijing and Shanghai) and industrialized areas of China (Hebei, Shandong, Henan, and Zhejiang province) is also shown, MRS.LEA is located in Gwangju, Korea.

ACPD
15, 3381–3413, 2015

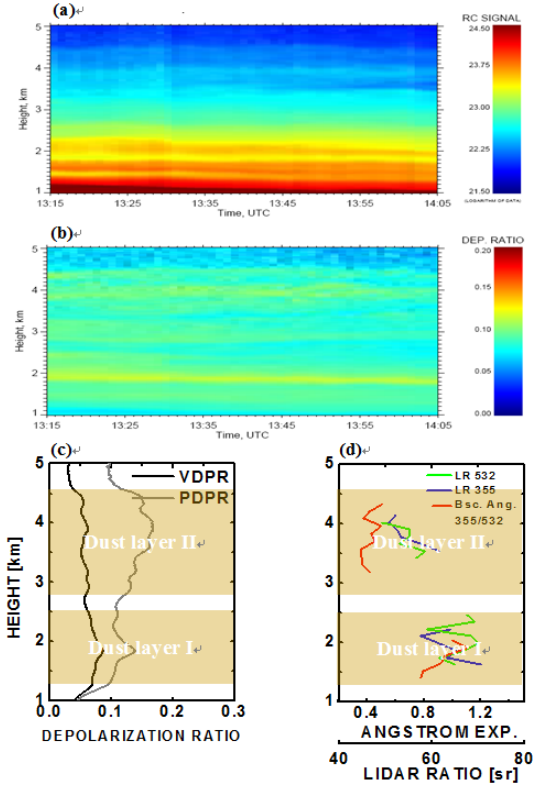

Figure 2. Measurement on 22 April 2012, 13:15–14:05 UTC. Shown are **(a)** the time-height cross section of the range-corrected signal and **(b)** the volume depolarization ratio at 532 nm. Also shown are the profiles of **(c)** the volume depolarization ratio and the particle depolarization ratio at 532 nm, and **(d)** the lidar ratio at 355 and 532 nm and the backscatter-related Ångström exponents.

ACPD
15, 3381–3413, 2015

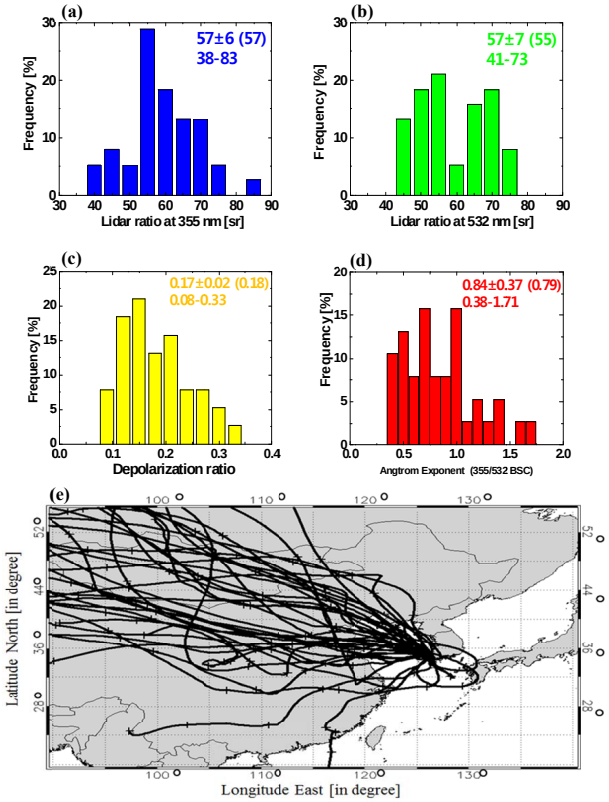

Figure 3. Frequency distributions of optical properties of Asian dust observed between 2009 and 2013. Shown are **(a, b)** lidar ratios at 355 and 532 nm, **(c)** linear particle depolarization ratios at 532 nm, and **(d)** Ångström exponents for the wavelength pair 355/532 nm. The numbers in each plot indicate the mean value and its SD, the median (shown in brackets), and the minimum and maximum value of each distribution. **(e)** Transport pathways of all Asian dust layers observed between 2009 and 2013. The HYSPLIT backward trajectories were calculated for 120 h transport time.

ACPD
15, 3381–3413, 2015

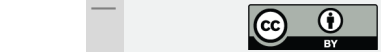

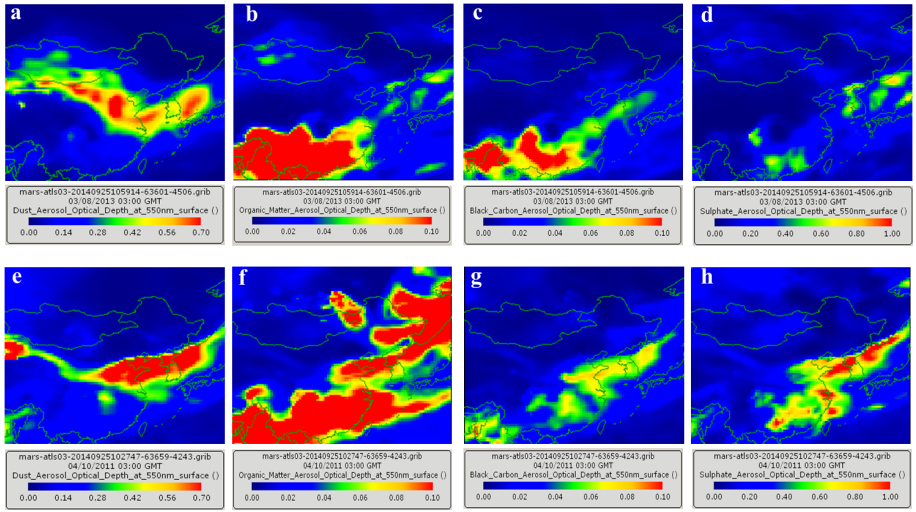

Figure 4. Distribution of AOD at 550 nm over East Asia retrieved from ECMWF for **(a)** and **(e)** dust, **(b)** and **(f)** organic matter, **(c)** and **(g)** black carbon, and **(d)** and **(h)** sulphate aerosol. **(a–d)** refers to 8 March 2013. That day is classified as a relatively "low polluted" day over East China. **(e–h)** refers to 10 April 2011 which is classified as a comparably "highly polluted" day over East China.

ACPD
15, 3381–3413, 2015

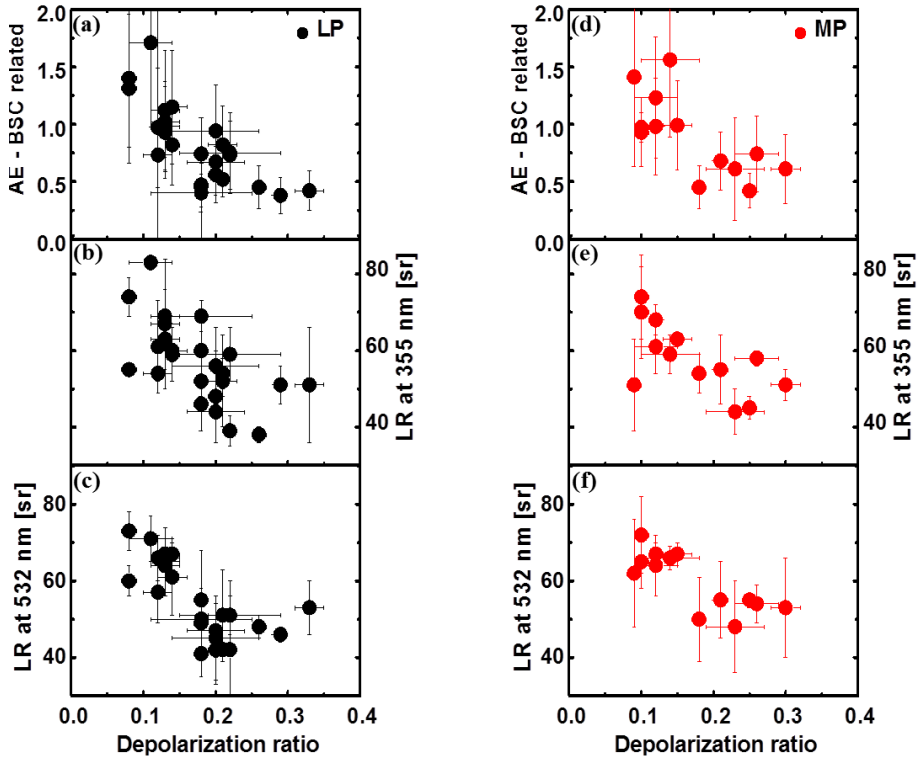

Figure 5. Scatter diagram of the linear particle depolarization at 532 nm vs. **(a)**, **(d)** the backscatter-related Ångström exponent (355/532 nm wavelength pair), **(b)**, **(e)** the lidar ratio at 355 nm and **(c)**, **(f)** the lidar ratio at 532 nm. The left column **(a–c)** shows the optical properties of Asian dust layers considered as less polluted (LP), the right column **(d–f)** shows the more polluted cases.

ACPD
15, 3381–3413, 2015

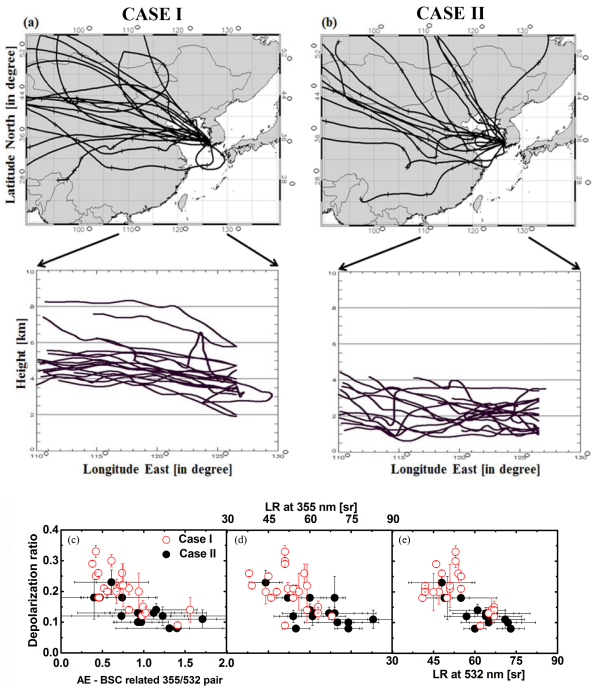

Figure 6. (top panel) Transport pattern of the dust plumes that originated in the desert regions and passed over industrialized/populated regions of China before arrival over the Korean peninsula. (middle panel) Vertical position of the dust layers during transport: **(a)** Dust layers passed over China at high altitude (Case I) **(b)** dust layers were transported over China through the near surface/lower troposphere (Case II). (bottom panel) Scatter diagram of the linear particle depolarization at 532 nm vs. **(c)** the backscatter-related Ångström exponent (355/532 nm wavelength pair), and the **(d, e)** lidar ratio (at 355 nm and at 532 nm) with respect to the Case I and Case II. The two categories I, II are denoted by different colors.

ACPD
15, 3381–3413, 2015

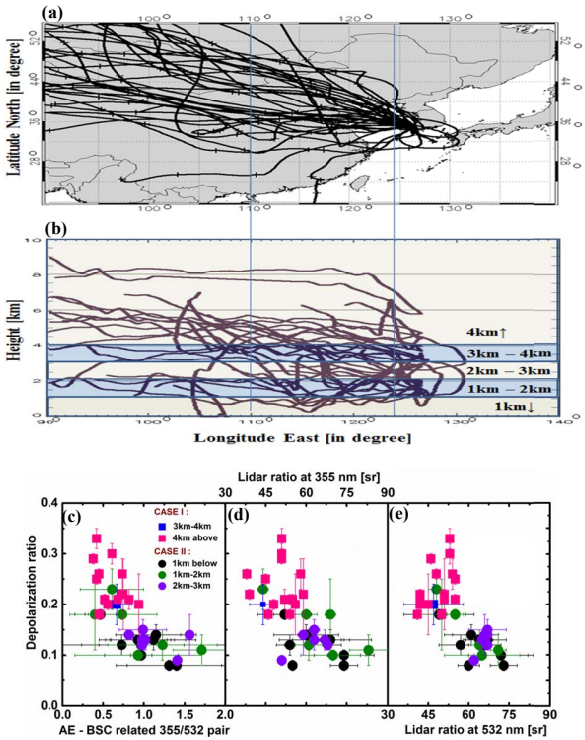

Figure 7. (Top panel) **(a)** The transport pathway and the classification of East Asian dust layers with respect to **(b)** their altitude above ground when they passed over industrial regions of China. (Bottom panel) Scatter plots of the linear particle depolarization at 532 nm vs. **(c)** the backscatter-related Ångström exponent (355/532 nm wavelength pair), vs. **(d)** the lidar ratio at 355 nm, respectively **(e)** the lidar ratio at 532 nm in dependence of the 5 altitude categories. The height of the Asian dust layers above ground is denoted by different colors and symbols. Case I included the layers from 3–4 km and above 4 km (blue and pink colored squares). Case II includes the layers from 0–1 km, from 1–2 km, and from 2–3 km height above ground (black, green and violet circles).

ACPD
15, 3381–3413, 2015

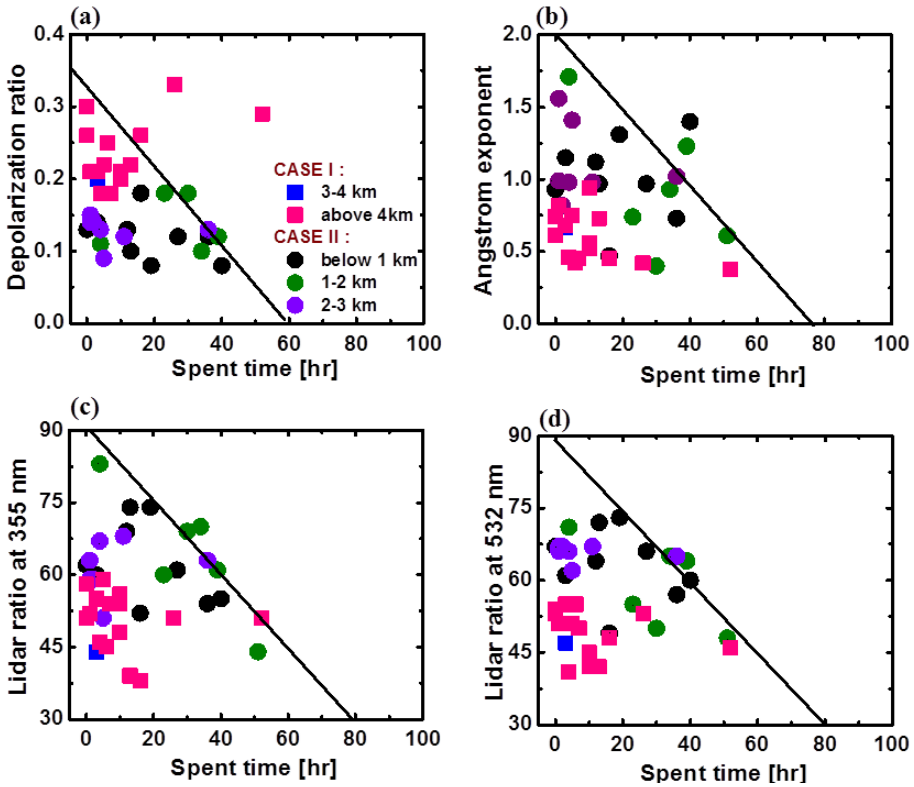

Figure 8. Scatter diagram of optical dust properties vs. the time the Asian dust layers travelled over polluted regions in China. Shown are **(a)** the particle depolarization ratio, **(b)** the backscatter-related Ångström exponent (355/532 nm wavelength pair), **(c)** the lidar ratio at 355 nm, and **(d)** the lidar ratio at 532 nm with respect to their altitude above ground when they passed over industrial regions of China. The meaning of the colors and symbols is the same as in Fig. 7.

ACPD
15, 3381–3413, 2015